Indian J. Phys. 71B (3), 223–243 (1997)

IJP B
— an international journal

High-resolution Excitation and Photoionization using Synchrotron Radiation from the Advanced Light Source

N. Berrah, B. Langer and A. Farhat

Physics Department, Western Michigan University
Kalamazoo, MI 49008, USA

Abstract: Fundamental aspects of atomic structure and the dynamics of the interaction of high-resolution photons with two-electron atoms and multielectron atoms has been measured. The emphasis of the reported work is on photoexcitation and photoionization of rare gas atoms and on near-threshold measurements following either outer-shell or inner-shell ionization. Specifically, He satellites, angular distribution of the Ar $3s^{-1} \rightarrow np$ (n = 4-16) autoionization resonances and the angular distribution of the Xe $4d_{5/2} \rightarrow 6p$ decay spectrum using the Auger resonant-Raman spectroscopy have been studied. The measurements were conducted using two newly-built third-generation time-of-flight (TOF) spectrometers coupled with unprecedented photon resolution from the Advanced Light Source. This third-generation synchrotron radiation source is a powerful tool since it can offer tunability, intensity, polarization and time structure. Presented results are compared with theories.

Keywords: photoexcitation, photoionization, synchrotron radiation, rare gas atoms, Auger resonant-Raman spectroscopy

PACS numbers: 32.80.Dz, 32.80.Fb, 32.80.Hd

1. Photoionization Near the He Double-Ionization Threshold

Photo-double-ionization is one of the fundamental processes of physics because it requires a solution of the three-body Coulomb problem where the boundary conditions for the two continuum electrons must be included. There has been much interest in the study of photo-double-ionization of He because it is a system that is dominated by electron-electron correlations. Because the independent electron model failed to provide adequate agreement with measurements, new theoretical approaches have had to be developed. Since the classic work of Wannier [1], numerous theoretical studies have been made on near-threshold ionization [2-4]. The various theories yield predictions for three different observable situations: (a) the energy dependence of the cross section (b) the energy sharing of the two outgoing electrons and (c) the angular correlation of these electrons. Wannier theory predicts, in the energy range just above threshold, that $\sigma^{++} = \sigma_0 E^{\alpha}_{exc}$. Kossmann et al. [5] made an extensive study of the threshold law for the cross section of double ionization in helium. Their results provide quantitative information about the Wannier exponent, $\alpha = 1.05\,(2)$ which agrees with the theoretical prediction of 1.056; a threshold value $\sigma_0 = 1.02\,(4) \times 10^{-21}\,\mathrm{cm}^2$ and $E_{th} = 79.013\,(10)$ eV. Furthermore, their experimental results find the range of validity of the cross-section threshold law to be approximately 2-eV excess energy above threshold. Lablanquie et al. [6] used coincidence measurements between low-energy electrons and doubly-charged ions to study the dynamics of double photoionization and confirmed the range of validity of the Wannier theory. They found that the energy distribution of the two outgoing electrons is flat, within 20%, in agreement with the theoretical prediction, but in a 15 eV energy range above threshold. Photoionization phenomena near the double-ionization threshold has also been extensively studied by Hall et al [7]. Using a photoelectron/photoion coincidence technique they find the value of the exponent α to be consistent with the Wannier prediction. They also investigate the behavior of the asymmetry parameter, β, near threshold and obtain a nearly constant value close to -0.4. Their result is in disagreement with the prediction of the Wannier theory which appears to underestimate the angular correlation between the two electrons [8]. Dawber et al. [9] have exploited the photoelectron-photoelectron coincidence technique to measure the triply-differential cross section (TDCS) at very low excess energies E ($0.6\ \mathrm{eV} < E < 2\ \mathrm{eV}$) for both equal and unequal energy sharing between the two outgoing electrons. The measured data are compared with the Wannier predictions and also with recent ab-initio calculations [10-12] that are not based on a Wannier-like treatment. Their measurements suggest a departure from the predictions of the Wannier model at the largest excess energy stud-

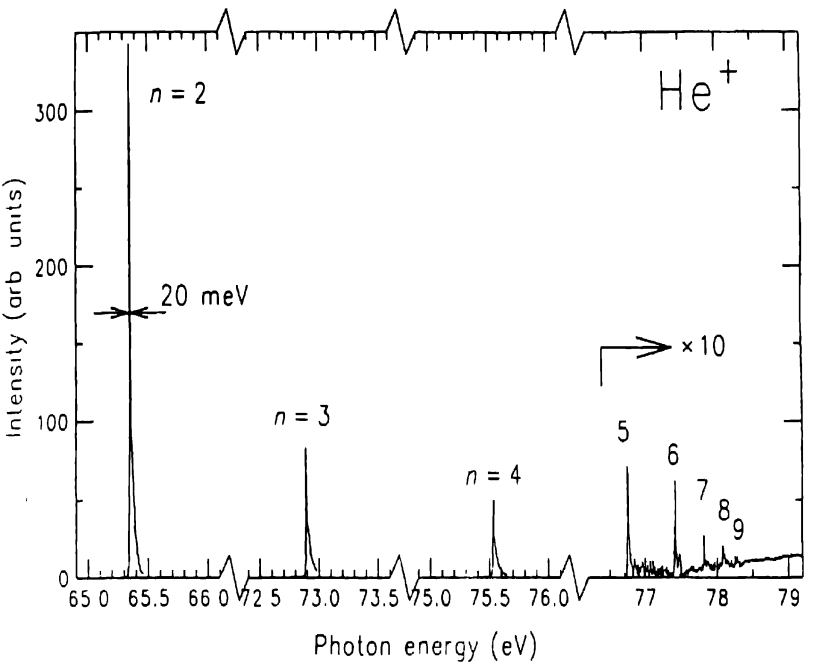

Fig. 1. Threshold spectrum obtained with a monochromator bandpass of 6 meV and photon energy increment of 5 meV.

ied, E = 2 eV. Lablanquie et al. [13] have also very recently studied the effect of electron energy sharing near the double-photoionization threshold. In their energy- and angle-resolved measurements, they observed that although the angular distributions do not depend much on the energy sharing of the two electrons at 4 eV above threshold, a strong effect is measured at E = 18.6 eV.

We have used a zero-volt spectrometer [14] to study with higher resolution than 50 meV [15] photoionization phenomena near the double-ionization threshold. Fig. 1 shows a preliminary spectrum taken with photons from an undulator beamline coupled with a spherical-grating monochromator of the Advanced Light Source (ALS) at Lawrence Berkeley Laboratory. The 1.5 GeV storage ring was filled to 40 mA in the two bunch mode at injection, and the monochromator bandpass was 6 meV near 79 eV. The scan in Fig.1 shows eight satellite lines which are the result of electron correlations. These satellite lines originate from an ionization process with additional excitation leaving the ion in a He^+ nl ($n > 1$) state. The linewidths are about 20 meV, an improvement by a factor of 2.5 over previous measurements [15]. Unfortunately,

when this experiment was carried out, the ALS experienced its first long-time failure to operate due to a serious obstruction in the beam path. This prevented us from total optimization of the spectrometer.

2. High-Resolution Angle-Resolved Photoelectron Spectroscopy: The Ar $3s^{-1} \rightarrow np$ (n = 4–16) Resonances

The discovery of a series of autoionizing states in He [16] and its explanation [17] were crucial for the understanding of electron-correlation effects. Theoretical work has shown that electron angular distributions [18] and the shape of autoionization resonances [19] are essential to understanding electron-electron correlations. Theoretical analysis [20] has shown that the angular distributions of photoelectrons in resonance regions are significantly different from those observed in non-resonance regions. The angular distribution can vary rapidly over an energy range on the order of a resonance width.

Accurate studies of electron angular-distributions parameters (β) are a sensitive probe [21] of atomic wave functions. According to Starace [22], dramatic changes in the parameter β is an indication of strong effects due to e-e correlations. The experimental determination of the anisotropy parameter β in the resonance region is an important source of information on the dynamics of resonance photoionization which cannot be obtained by absorption or ion mass spectrometry.

Autoionization resonances studied in this work result from the decay of the excited discrete states Ar^* $3s3p^6$ np into the continuum state Ar^+ $3s^23p^5$ + e^- (ks,kd). Because the continuum also can be reached by direct photoionization, the two paths give rise to interference effect that produce the characteristic Beutler-Fano line shape [23]. Detailed measurements of the shape of this autoionization series were conducted previously using absorption techniques [24] and ion mass spectrometry [25]. Also, angular distributions for the first three autoionization resonances have been measured using photoelectron spectrometry [26]. These autoionization resonances have been calculated using many-body perturbation theory [27], multichannel quantum-defect theory [28], the eigenchannel R-matrix method [29], the K-matrix procedure [30], and the random-phase approximation with exchange [31].

We have measured detailed high-precision angle-resolved electron-spectrometry measurements of the Ar $3s^23p^6 \rightarrow 3s3p^6$ np (n = 4-16) autoionization resonances in the energy range between 26 and 29.3 eV. The aim of this work was to provide a critical test of present calculations and a testing ground for further theoretical advances. We have taken advantage of the high resolution and high brightness of an undulator beamline at the ALS, coupled

with our electron time-of-flight spectrometers, to obtain for the first time (1) accurate measurements of the photoelectron angular-distribution parameters for all members of the series and (2) first observation from $n = 8$ to $n = 16$ of the Ar $3s^2 3p^6 \rightarrow 3s3p^6$ Rydberg series. We have fit the angular-distribution data using a model function derived by Kabachnik and Sazhina [32] and the comparison of our results with the R-matrix calculations of Taylor [18] and our R-matrix calculations is found to be excellent. We also have analyzed the cross-section shape of each resonance, using a model function originally given by Fano [33], and have determined the values of the shape parameter q, the correlation parameter ρ^2 and the resonance width Γ of the Beutler-Fano profiles which best describe them. Our results confirm previous measurements [24,25] for the lower 6 resonances.

Experimental Procedure.

Two components of instrumentation were essential in these high-resolution gas-phase photoemission measurements: (1) a monochromator with a resolving power $E/\Delta E$ of at least 10,000, and (2) an angle-resolved technique to measure angular distributions. The experiment was carried out with our newly-built apparatus, similar in design to previous ones [35], but equipped with upgraded and advanced TOFs. Briefly, it consists of a rotating vacuum chamber that houses two advanced time-of-flight (TOF) spectrometers [36] to record spectra simultaneously and to allow both partial-cross section and angular-distribution measurements. The two TOFs are mounted perpendicular to the incoming photon beam with a 0.99 linear polarization, as shown in Fig. 2. Details of the experimental apparatus are described in a previous reference [36]. Fig. 3 shows one of our scans of the Ar $3s^2 3p^6 \rightarrow 3s3p^6\, np$ Rydberg series of window type resonances from $n = 4$ to $n = 16$, measured at an angle of 0° and at the magic angle with respect to the electric-field vector of the linearly-polarized synchrotron beam.

Theoretical background

In the dipole approximation, valid for low-energy photons, $h\nu$, the differential photoionization cross section, $d\sigma_{if}/d\Omega$, and the photoelectron angular-distribution parameter, β, resulting from photoionization of state $|i\rangle$ by linearly-polarized photons leaving the ions in state $|f\rangle$ is given by [37]:

$$\frac{d\sigma_{if}}{d\Omega} = \frac{\sigma_{if}}{4\pi} \left[1 + \beta_{if} P_2(\cos\theta)\right] \qquad (1)$$

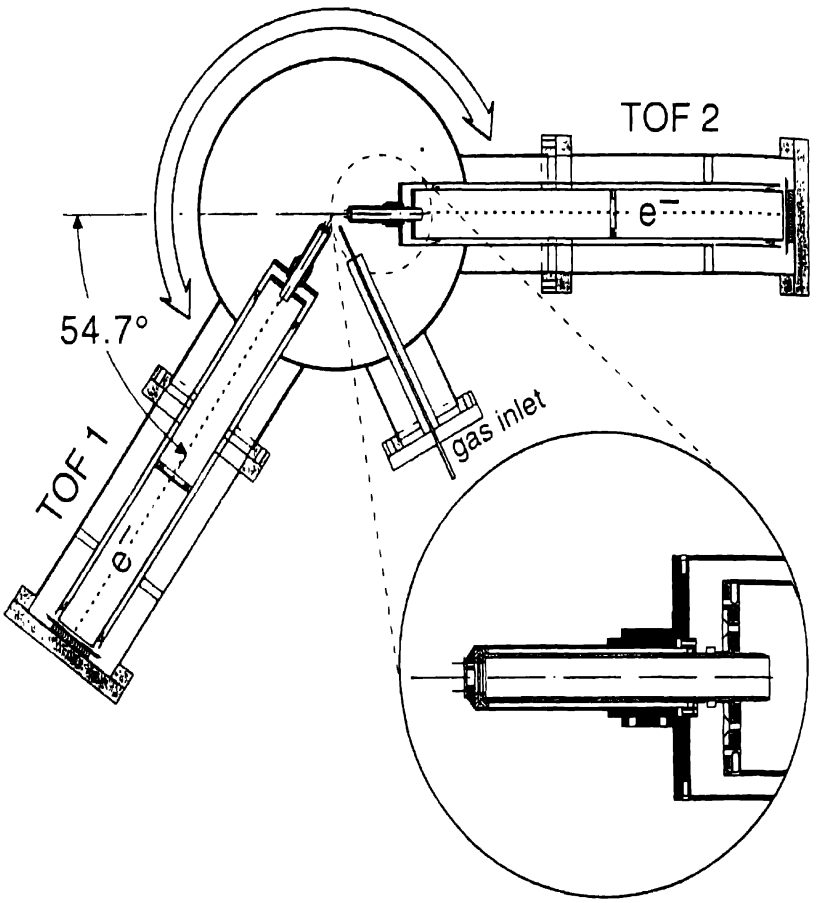

Fig. 2. Schematic diagram of the apparatus showing the interaction region in the rotating chamber that houses two TOF spectrometers. The photon beam is perpendicular to the drawing plane.

where σ_{if} is the total photoionization cross section for producing state $|f\rangle$ of the ion, θ is the angle between the photon polarization vector and the photoelectron momentum direction, $P_2(x) = (3x^2 - 1)/2$, and β_{if} is the electron angular-distribution parameter.

We have used a parameterization of the variation in β_{if} over autoionizing resonances introduced by Kabachnik and Sazhina [32]. It is based on the Fano [33] parameterization for the total photoionization cross section, σ_{if}, given by [18]:

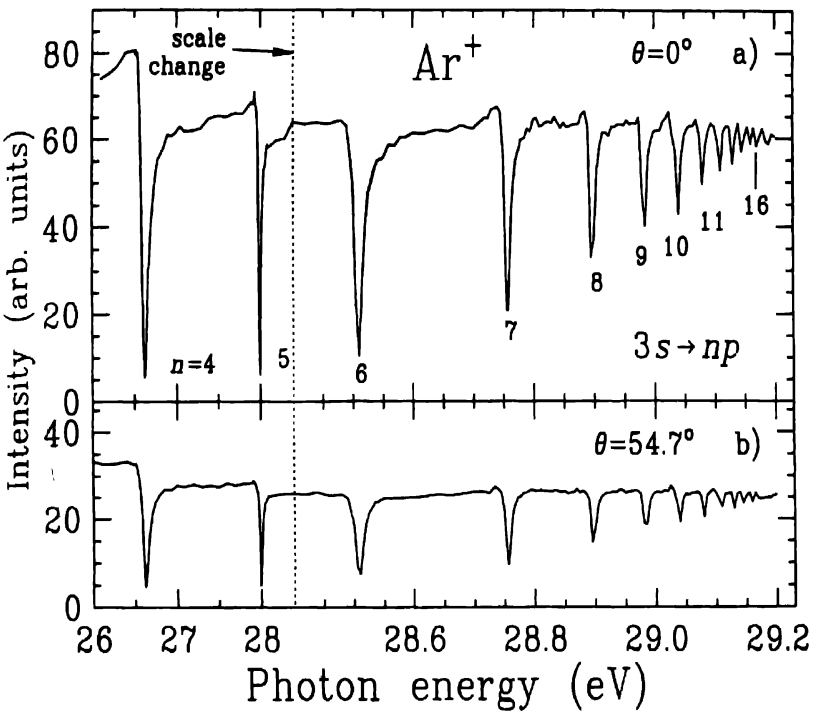

Fig. 3. Photoelectron yield scan of the Ar $3s^2 3p^6 \rightarrow 3s3p^6 np$ autoionization resonances at 0° and at the magic angle with respect to the polarization of the synchrotron light.

$$\sigma = \sigma_a \frac{(q+\varepsilon)^2}{(1+\varepsilon^2)} + \sigma_b \tag{2}$$

where q is the line-profile index and ε is given by:

$$\varepsilon = \frac{E - E_r}{\Gamma/2} \tag{3}$$

and

$$\rho^2 = \frac{\sigma_a}{\sigma_a + \sigma_b} \tag{4}$$

where E_r is the position of the resonance and Γ its width. The cross sections σ_a and σ_b are slowly varying background cross sections. Also derived [32,18] is the expression for β given by:

$$\beta = -2\,\frac{X\varepsilon^2 + Y\varepsilon + Z}{A\varepsilon^2 + B\varepsilon + C} \tag{5}$$

with:

$$A = \frac{\sigma_a + \sigma_b}{4\pi},\ B = \frac{2q\sigma_a}{4\pi},\ C = \frac{\sigma_a q^2 + \sigma_b}{4\pi}, \tag{6}$$

with X, Y, and Z considered as free parameters in the fit to the data.

Results and Discussion

The variation of β as a function of photon energy is shown in Fig. 4. These scans were obtained using two simultaneously recorded electron-yield signals at $\theta = 0°$ and at the magic angle, $\theta = 54.7°$. We have fit the above expressions to both the angular distribution and to total photoionization cross section data. The angular-distribution data compared with the fit based on the parameterization [38] gave a very good accord as shown in Table 1.

The angular-distribution data was also compared to the untested theory of Taylor [18] based on the R-matrix method listed in Table 1. Taylor used in the first approximation a single-configuration (SC) wavefunction to represent the $^2P^0$ and $^2S^e$ ionic states of the direct and indirect photoionization paths. He also made a more sophisticated approximation [38] (CI) where multiconfigurational wavefunctions are used in the representation of these states. Both calculations were done in the length and velocity form. The CI calculations improved the agreement between the length and velocity results for the only two calculated resonances $n = 4$ and $n = 5$ by Taylor [18]; the length and velocity results were coincident. Comparison of the $n = 4, 5$ resonances with the CI calculation of Taylor is shown in Fig. 5a,b along with our R-matrix calculations [39] performed by Gorczyca. In all cases, the dotted lines are deconvoluted fits (6 meV). As can be seen, agreement between the data and both theories is excellent. The parameters X, Y, and Z produced by our fit were compared for $n = 4$ and $n = 5$ with the results from Taylor as shown in Table 1. The CI calculation was indeed a better model for the data because, in the case of $n = 4$, the SC calculation did not even predict the correct sign of the Y parameter. Excellent agreement between the data and the

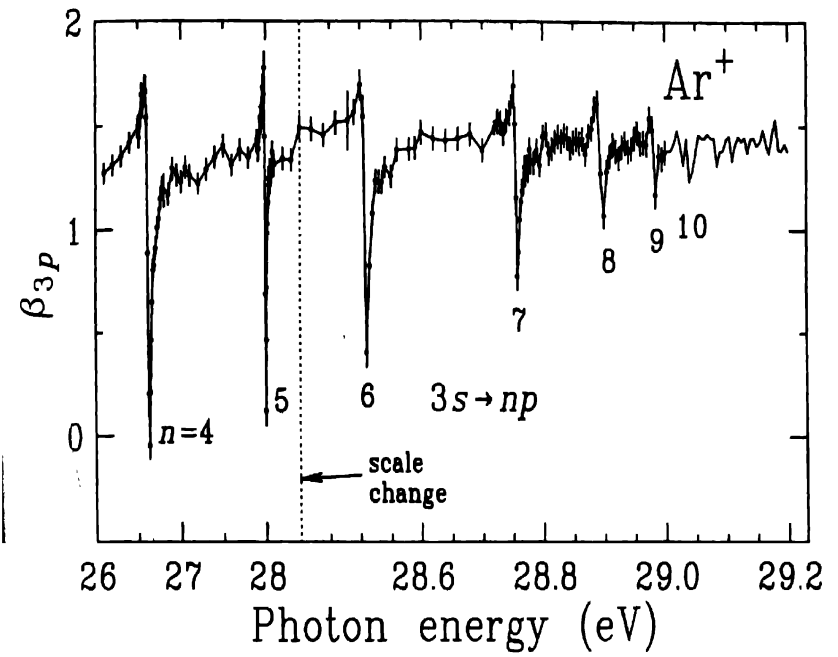

Fig. 4. Angular-distribution of the anisotropy-parameter b measurements of the Ar $3s^2 3p^6 \rightarrow 3s 3p^6\, np$ autoionization resonances.

CI calculations was found.

We also fit the total photoionization cross-section data using the above expressions and extracted the fitting parameters, the width Γ, the line profile q and the correlation coefficient ρ^2, for the photoionization cross section in the region of the first six resonances. Our results, listed in Table 2, are in good agreement with previous quantitative measurements [28,29] and calculations by Burke and Taylor [38]. There is excellent agreement with Burke and Taylor's CI theory, in particular, in the case of $n = 4$, one observes that the CI theory agrees very well, while the SC calculation and multiconfiguration Dirac-Fock (MCDF) calculation of Tulkki's [25] theory agree with each other but not with the data.

3. Angular Distribution of the Xe $4d_{5/2} \rightarrow 6p$ Decay Spectrum using the Auger Resonant-Raman Spectroscopy

Auger resonant-Raman [40] spectroscopy is a powerful tool for studying the resonant Auger decay processes with a resolution narrower than the

Table 1. Profile parameters for the first nine members of the $3s3p^6\,np$ series resonances compared with previous measurements and calculations.

	$3s\rightarrow4p$				$3s\rightarrow5p$				$3s\rightarrow6p$			
Method	Pos. (eV)	Γ (meV)	q	ρ^2	Pos. (eV)	Γ (meV)	q	ρ^2	Pos (eV)	Γ (meV)	q	ρ^2
R-Matrix & CI (L)[a]		68	-0 33	0.855		24 3	-0.26	0.85				
R-Matrix & CI (V)[a]			-0.29	0.861			-0 22	0.86				
RPAE[b]		85	-0.27	0.89								
MCDF[c]		12	-0.70	0.24							-0.262	0.824
R-Matrix & CI (L)[d]	26 633	83.8	-0.383	0.843	27 997	2[illegible]	-0 292	0.825	28.508	12.4	-0.312	0.827
R-Matrix & CI (V)[d]			-0 433	0 846			-0.342	0.829				
absorption[e]	26 616	80(5)	-0.22(5)	0.86(4)	27.998	28 2(13)	-0 21(2)	0 83(2)	28.511	12.6(12)	-0.17(3)	0.85(3)
ion yield[c]	26.606	76(5)	-0.249(3)	0 890(5)	27.993	25(7)	-0.168(5)	0.873(7)	28.506	16(7)	-0.200(5)	0.526(7)
electron yield[d]	26.608	80.3(7)	-0.286(4)	0.840(3)	27.994	28 5(3)	-0.177(3)	0 848(3)	28.507	12.2(3)	-0.135(9)	0 852(9)

	$3s\rightarrow7p$				$3s\rightarrow8p$				$3s\rightarrow9p$			
	Pos. (eV)	Γ (meV)	q	ρ^2	Pos. (eV)	Γ (meV)	q	ρ^2	Pos. (eV)	Γ (meV)	q	ρ^2
R-Matrix & CI (L)[d]	28.756	6.65	-0.249	0.823	28.896	3.97	-0.240	0.824	28.982	2.57	-0.235	0.823
R-Matrix & CI (V)[d]		6.66	-0.299	0.827			-0.291	0.827			-0.286	0.826
ion yield[c]	28.757	9(7)	-0.129(6)	0 453(8)	28.898	10(10)	-0 104(3)	0.38(1)				
electron yield[d]	28.755	6.6(1)	-0.125(4)	0.846(9)	28.896	4 5(2)	-0.132(4)	0.77(2)	28.982	4.1(2)	-0.115(8)	0.63(3)

a. Burke and Taylor [38]
b. Amusia and Kheifets [21]
c. Sorensen *et al.* [25]
d. Present results
e. Madden, Ederer, and Codling [24]

Table 2. Comparison of the fitted (solid line through the data) and calculated angular-distribution parameters for the $3s3p^6 4p$ and $5p$ resonances in Ar.

Method	$3s \rightarrow 4p$			$3s \rightarrow 5p$			$3s \rightarrow 6p$		
	X	Y	Z	X	Y	Z	X	Y	Z
R-Matrix & SC(L)[a]	−1.53	−2.88	−1.21						
R-Matrix & SC(V)[a]	−0.81	−0.81	−0.09						
R-Matrix & CI (L)[a]	-1.79	1.85	-0.44	-1 77	1.33	-0.14			
R-Matrix & CI (V)[a]	-1.47	1.44	-0.31	-1.46	1.01	-0.06			
R-Matrix & CI (L)[b]	-1.73	1.99	-0.56	-1.67	1.55	-0.41	-1.66	1.40	-0.34
R-Matrix & CI (V)[b]	-1.41	1.73	-0.54	-1.36	1.35	-0.39	1.35	1.22	-0.32
electron yield[b]	-1.567(12)	1.49(2)	-0.322(12)	-1.483(11)	1.00(2)	-0.158(13)	-1.46(2)	0.95(4)	-0.10(2)
	$3s \rightarrow 7p$			$3s \rightarrow 8p$			$3s \rightarrow 9p$		
	X	Y	Z	X	Y	Z	X	Y	X
R-Matrix & CI (L)[b]	-1.65	1.36	-0.35	-1.64	1.22	-0.26	-1.63	1.29	-0.33
R-Matrix & CI (V)[b]	-1.34	1.19	-0.33	-1.33	1.08	-0.25	-1.32	1.13	-0.31
electron yield[b]	-1.507(10)	0.97(4)	-0.15(3)	-1.489(14)	0.79(7)	-0.13(6)	-1.49(2)	0.56(9)	-0.46(8)

a. Taylor [18]
b. Present results

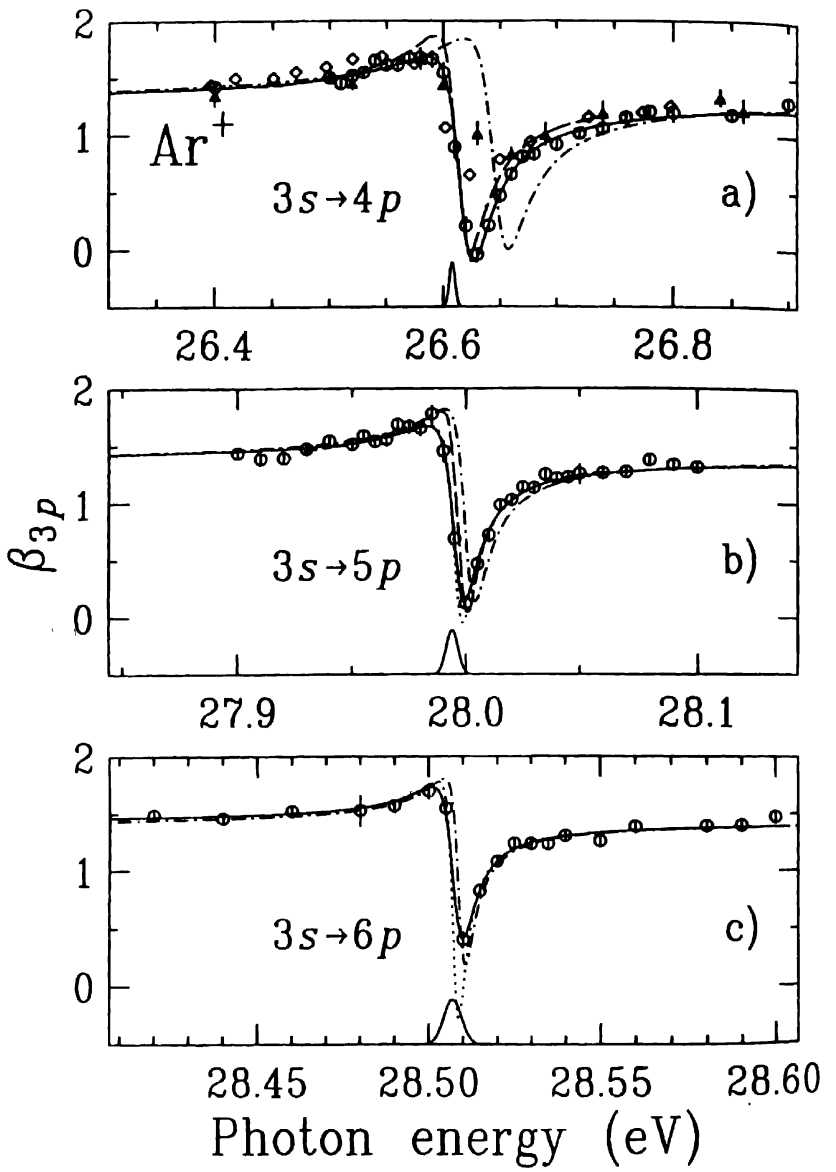

Fig. 5a. Angular distribution of the Ar $3s^2 3p^6 \rightarrow 3s3p^6\, np$ autoionization resonances fitted to Kabachnik and Sazhina model [32]. The dotted lines are deconvoluted fits. The circle are the present data and the triangles are Ref. [26]. The solid line is our fit. The dashed line is Ref. [18] and the dotted dashed is our calculations not shifted to fit the position of the resonance unlike Ref. [18].

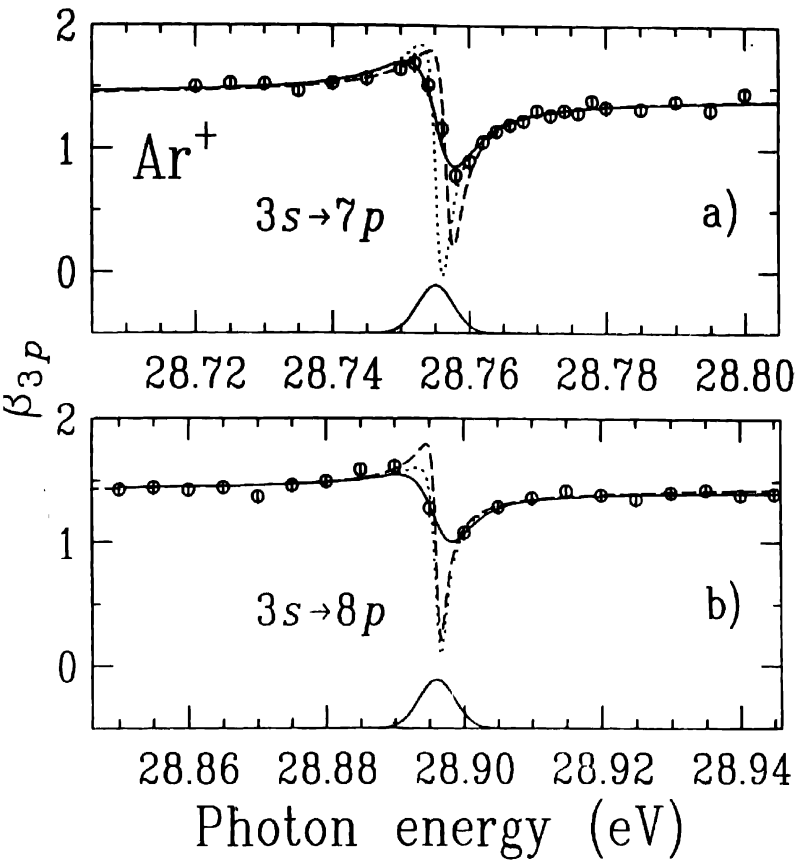

Fig. 5b Same as Fig. 5a.

natural lifetime width of the initial inner-shell hole state [41]. This effect has been used to analyze branching ratios of resonantly excited atoms [42,43] and molecules [44]. Here, we report on results of a study of the angular distributions of the spectator decay lines of Xe following $4d_{5/2} \rightarrow 6p$ excitation using the Auger resonant-Raman effect and highly resolved photons from the ALS.

The resonant Auger decay spectrum of the Xe $4d_{5/2} \rightarrow 6p$ resonance was first reported by Eberhardt et al. in 1978 [45] followed by other experimental and theoretical studies [46-51]. It took more than a decade after the first observation until measurements on the angular distribution were performed by Carlson et al. [52], who found anomalously negative β-values in the decay spectrum. Such behavior was first explained theoretically for the

decay of the Ar $2p \rightarrow 4s$ resonance by Cooper [53], who applied angular-momentum-transfer theory, treating the resonant decay as a single-step process. Kämmerling et al. [54] compared resonant-Auger and normal-Auger angular distributions experimentally and theoretically. These experimental studies were limited by the low resolution of the photon sources as well as of the electron spectrometers, making it difficult to compare the results with the various theoretical calculations [53-58].

Recently, however, the development of new synchrotron sources and high-resolution monochromators in combination with high-resolution electron spectrometers has made it possible to study the energy positions and intensities of the peaks in the Xe $4d_{5/2} \rightarrow 6p$ decay spectrum with a resolution better than the natural linewidth (106 meV [59]) of the $4d$ inner-shell hole by utilizing the Auger resonant-Raman effect [42,43]. Using this technique, we are now able to determine the angular distribution parameters β of almost all of the possible final ionic $5p^4(^3P,^1D,^1S)6p$ states.

After a Xe $4d \rightarrow 6p$ excitation the decay process can involve 1) an excited electron (participator decay) resulting in an enhancement of the $5p$-1 or $5s$-1 main lines or 2) an excited $6p$ electron that remains in its state during the decay process (spectator decay) leaving the ion in a two-hole, one-electron (satellite) state. The spectator decay is the dominant process (57%), followed by simultaneous emission of two electrons (shake-off), leaving almost no intensity for the participator decay [50]. During the decay, the excited $6p$ electron can also move into the $7p$ orbital (shake-up) enhancing the $5p^4 7p$ final states. In the present study we focused on the strongest spectator decay channels, $5p^4(^3P,^1D,^1S)6p$ as shown in Fig. 6 and Fig. 7.

The experiment was performed at the ALS in conditions similar to the previous section. Fig. 1 shows electron spectra taken simultaneously at different angles ($\theta = 0°, 54.7°$) by two time-of-flight (TOF) spectrometers, which were mounted on a rotatable chamber. A retarding voltage was applied to the spectrometers to increase the flight time of the electrons and therefore improve their energy resolution. Fig. 2 shows a section of the decay spectrum recorded with a 32 V retarding potential at three different angles ($\theta = 0°, 54.7°, 90°$).

The results for the relative intensities and the angular distribution parameters β are shown in Table 3, together with theoretical calculations from Tulkki et al. [58], Chen [57], and Hergenhahn et al. [55,56]. Chen, Tulkki et al., and Hergenhahn et al. [56] used a multiconfiguration Dirac-Fock (MCDF) method in intermediate coupling with configuration interaction, whereas the older calculations of Hergenhahn et al. [55] were carried out in jK coupling applying a strict spectator model. Only Tulkki et al. include

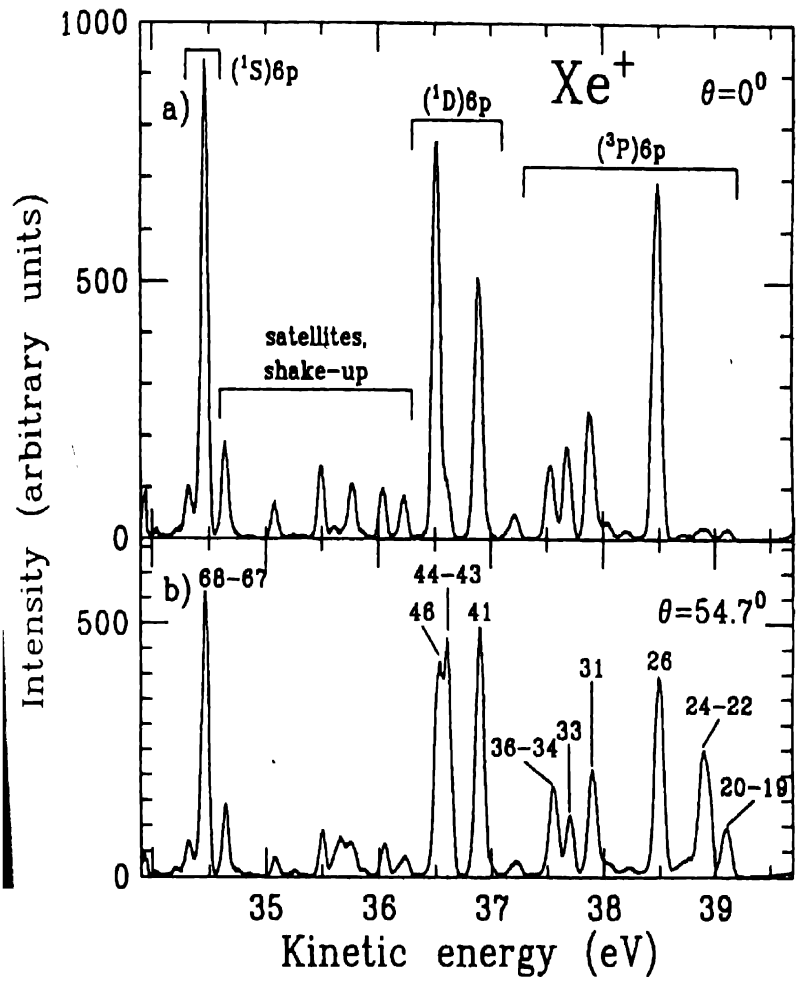

Fig. 6. Xe $5p^4\ nl$ decay spectra after $4d_{5/2} \rightarrow 6p$ resonant excitation at a) 0° and b) 54.7° with respect to the polarization of the incident photons. The spectra were recorded with a 30-V retarding potential which corresponds to a spectrometer resolution of between 45 and 70 meV in the displayed region.

exchange with different continuum channels in their calculations. All the theoretical calculations have in common that both the direct photoionization and the participator decay are neglected, and these approximations have been verified experimentally [47,48].

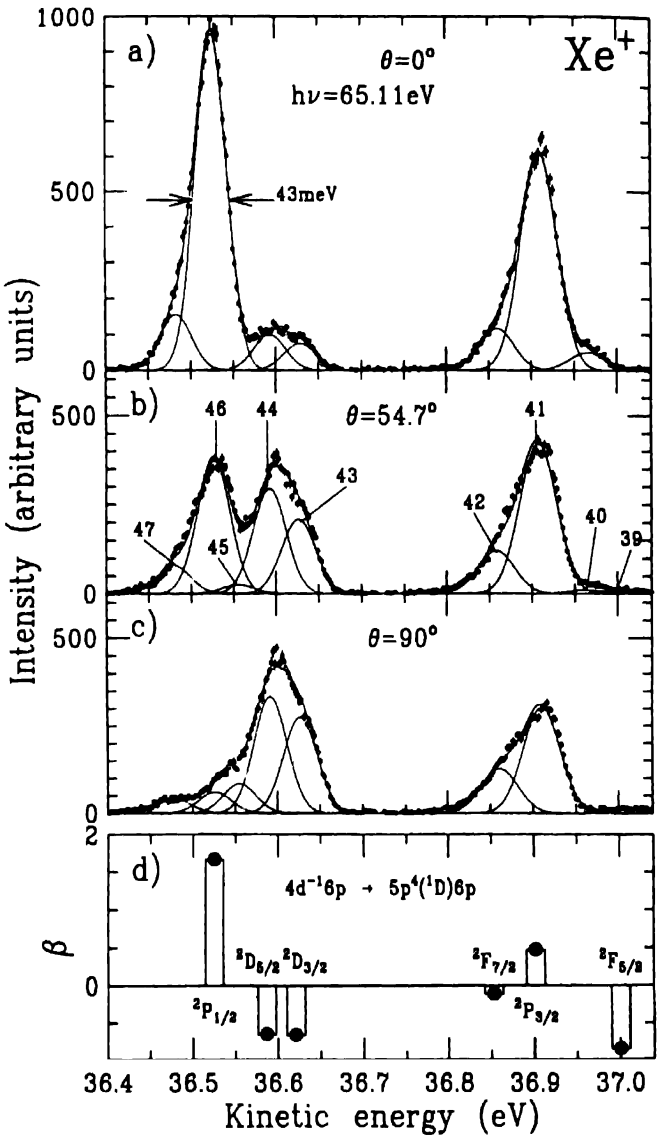

Fig. 7. Xe $5p^4\,nl$ decay spectra after $4d_{5/2} \rightarrow 6p$ resonant excitation in the kinetic energy range of 36.4-37.1 eV at a) 0°, b) 54.7°, and c) 90° with respect to the polarization of the incident photons. The spectra were measured with a 32-V retarding potential corresponding to a spectrometer resolution of between 43 and 50 meV in the displayed region. Part d) shows the angular distribution parameter β for the $5p^4$ (^1D) $6p$ spectator lines.

Table 3. Intensities and β parameters of the electron spectrum of Xe after $4d_{5/2} \rightarrow 6p_{3/2}$ excitation (65.110 eV). Intensities are normalized relative to the well separated $(^3P)6p(^2P_{3/2})$ line (line 26). The statistical uncertainty of the last digits is given in brackets. The identification of the peaks from Chen [57] was done with respect to the calculated energies.

Final ionic state		Line in experiment[b]	Kinetic energy (eV)[b]	Relative intensity	β	β theory[a]			
Term[b]						Ref [58]	Ref [57]	Ref [56]	Ref [55]
$5p^4(^3P)6p$	$^4P_{3/2}$	19	39.119	2.0(5)	1.4(6)	1.045	0.984	0.061	1.014
$(^3P)6p$	$^4P_{5/2}$	20	39.098	23.2(7)	-0.85(3)	-0.994	-1.000	-0.999	-0.998
$(^3P)6s$	$^2D_{3/2}$	21[c]	38.975	0.82(12)	2.0(3)				
$(^3P)6p$	$^2D_{5/2}$	22	38.906	37.5(8)	-0.967(12)	-0.994	-1.000	-1.000	-0.998
$(^3P)6p$	$^2S_{1/2}$	23	38.886	17.1(6)	-0.69(3)	-0.448	0.215[e]	0.157[e]	0.451[e]
$(^3P)6p$	$^4D_{7/2}$	24	38.882			-0.588	-0.974	-0.923	-0.932
$(^1D)5d$	$^2G_{9/2,7/2}$	25[c]	38.738	4.0(2)	-0.16(3)				
$(^3P)6p$	$^2P_{3/2}$	26	38.501	100	1.30(2)	1.030	1.018	0.972	1.014
$(^1D)5d$	$^2F_{5/2}$	27[c]	38.216	2.9(2)	0.60(11)				
$(^3P)6p$	$^2P_{1/2}$	28	37.988	5.0(2)	1.03(7)	0.984	0.962[e]	0.749[e]	n. a.[d,e]
$(^3P)6p$	$^4P_{1/2}$	30	37.955	7.1(3)	-0.13(6)	0.233	0.774[e]	0.927	1.000
$(^3P)6p$	$^2D_{3/2}$	31	37.899	42.8(5)	0.73(3)	0.656	0.653[e]	0.910[e]	0.800[e]
$(^3P)6p$	$^4D_{5/2}$	32	37.716	1.3(4)	0.3(6)	-0.188	-0.331	-0.321	0.737
$(^3P)6p$	$^4S_{3/2}$	33	37.627	24.0(6)	1.13(5)	0.745[e]	0.955	0.557	-0.861
$(^3P)6p$	$^4D_{3/2}$	34	37.570	22.1(5)	-0.14(3)	-0.536[e]	-0.860[e]	-0.764[e]	-0.861[e]
$(^3P)5d$	$^2G_{5/2}$	35[c]	37.567						
$(^3P)6p$	$^4D_{1/2}$	36	37.535	19.5(4)	0.52(3)	0.593	0.935[e]	0.817[e]	1.000[e]
$(^1D)5d$	$^2P_{1/2}$	37[c]	37.232	5.6(2)	1.36(6)				
$(^1D)5d$	$^2D_{3/2}$	38[c]	37.169	2.7(2)	0.69(11)				
$(^1D)6p$	$^2F_{5/2}$	39	37.001	2.10(14)	-0.85(10)	-0.875	0.860	-0.914	-0.928
$(^1D)6s$	$^2S_{1/2}$	40[c]	36.959[e]	3.0(2)	2.0(3)				
$(^1D)6p$	$^2P_{3/2}$	41	36.902	82.7(10)	0.47(2)	0.175	0.073	-0.319	-0.399
$(^1D)6p$	$^2F_{7/2}$	42	36.853	24.3(5)	-0.11(3)	0.246	0.052	0.116	0.112
$(^1D)6p$	$^2D_{3/2}$	43	36.621	39.0(7)	-0.66(2)	-0.553	-0.529	-0.375	-0.399
$(^1D)6p$	$^2D_{5/2}$	44	36.587	51.0(8)	-0.65(2)	-0.888	-0.882	-0.930	-0.928
$(^3P)7s$	$^4P_{5/2}$	45[c]	36.550	6(1)	s. n.[f]				
$(^1D)6p$	$^2P_{1/2}$	46	36.521	63.1(6)	1.66(2)	1.503	1.307	0.550	0.373
$(^3P)7s$	$^2P_{3/2}$	47[c]	36.232	13.9(3)	0.94(4)				
$(^1S)6p$	$^2P_{1/2}$	65	34.602	1.6(3)	0.73(4)	0.130	-0.139	-0.035	n. a.[d]
$(^1S)6p$	$^2P_{3/2}$	67 68	34.479 34.456	98.9(6)	1.17(4)	0.829	0.847	0.754	0.800

a The originally-given α_2 values are multiplied by $-\sqrt{2}$

b According to Aksela *et al.* [43]

c. Satellite line.

d. Not allowed.

e Energy taken from Hansen and Persson [60]

f Strongly negative

Comparing our results to the different calculations, we find that the agreement varies between excellent and poor, depending of the configuration and method used. For some lines (20, 22, 31, 39) there is excellent agreement and for others (24, 43, 44) good agreement between our experimental anisotropy parameters and the results from all four calculations. For other lines (30, 34, 41, 65) the theoretical values are in disagreement with each other and with our experimental values. Finally, there are some configurations where our data agree with one or the other calculation. For instance, Chen [57] comes close to our β value for the $(^3P)6p(^4S_{3/2})$ state (line 33), whereas Tulkki et al. and Hergenhahn et al. [55] do not even have the correct sign. On the other hand, for the $(^3P)6p(^4D_{1/2})$ peak (line 36), Tulkki et al. give almost the same β value as the experiment but the other calculations are off. Interestingly, there is almost perfect agreement between all theories for our reference peak $(^3P)6p(^2P_{3/2})$ (line 26), but the experimental β value is significantly larger. We were able to observe the splitting of the $(^1S)6p(^2P_{3/2})$ state (lines 67 and 68), as Aksela et al. [43] did, but the fitting procedure was very sensitive to even small changes in the positions and widths of the peaks. Therefore, in Table 3 we give only the average β for those lines.

Acknowledgments

We wish to thank Andreas Hempelmann and Uwe Becker for their zero-volt spectrometer and the ALS, funded by DoE, for providing the source of photons. BL is indebted to the Alexander von Humboldt Foundation for partial financial support. This work was supported by the US Department of Energy, Office of Basic Energy Science, Division of Chemical Science, under contract No. DE-FG02-92ER14299.

References

[1] G. H. Wannier, Phys. Rev. **90**, 817 (1953).

[2] A. R. P. Rau, Phys. Rev. A **4**, 207 (1971).

[3] H. Klar and W. Schlecht, J. Phys. B **9**, 1699 (1976).

[4] C. H. Greene and A. R. P. Rau, Phys. Rev. Lett. **48**, 533 (1982).

[5] H. Kossmann, V. Schmidt and T. Andersen, Phys. Rev. Lett. **60**, 1266 (1988).

[6] P. Lablanquie, K. Ito, P. Morin, I. Nenner and J. H. D. Eland, Z. Phys. D **16**, 77 (1990).

[7] R. I. Hall, A. G. McConkey, L. Avaldi, K. Ellis, M. A. MacDonald, I. Dawber and G. C. King,. J. Phys. B **25**, 1195 (1992).

[8] G. Dawber, R. I. Hall, A. G. McConkey, M. A. MacDonald and G. C. King, J. Phys. B **27**, L341 (1994).

[9] G. Dawber, L. Avaldi, A. G. McConkey, H. Rojas, M. A. MacDonald and G. C. King, J. Phys. B **28**, L271 (1995).

[10] A. Huetz, P. Selles, D. Waymel and J. Mazeau, J. Phys. B **24**, 1917 (1991).

[11] A. Kazansky and V. N. Ostrovski, J. Phys. B **27**, 447 (1994).

[12] F. Maulbetsch and J. S. Briggs, Phys. Rev. Lett. **68**, 2004 (1994).

[13] P. Lablanquie, J. Mazeau, L. Andric, P. Selles and A. Huetz, Phys. Rev. Lett. **74**, 2192 (1995).

[14] F. Heiser, U. Hergenhahn, J. Viefhaus, K. Wieliczek and U. Becke, J. Electron Spectrosc. Relat. Phenom. **60**, 337 (1992).

[15] R. I. Hall, L. Avaldi, G. Dawber, M. Zubek, K. Ellis and G. C. King, J. Phys. B **24**, 115 (1991).

[16] R. P. Madden and K. Codling, Phys. Rev. Lett. 516 (1963).

[17] J. W. Cooper, U. Fano and F. Prats, Phys. Rev. Lett. **10**, 518 (1963)

[18] K. T. Taylor, J. Phys. B **10**, L699 (1977).

[19] H. Feshback, Ann. Phys. **19**, 287 (1962).

[20] V. V. Balashov, N. M. Kabachnik, I. P. Sazhina, Proc. 5th Sov. Conf. on Physics of Electronic and Atomic Collisions (Uzhgorod:Nauka) p.118

[21] M. Ya. Amusia and A. S. Kheifets, Phys. Lett. **82A**, 407 (1981).

[22] A. F. Starace, Phys. Rev. A **16**, 231 (1977).

[23] H. Beutler, Z. Phys. **93**, 177 (1935).

[24] R. P. Madden, D. L. Ederer and K. Codling, Phys. Rev. **177**, 136 (1969); M. A. Baig and M. Ohno, Z. Phys. D **3**, 369 (1986).

[25] S. L. Sorensen, T. Aberg, J. Tulkki, E. Rachlew-Källne, G. Sundström and M. Kirm, Phys. Rev. A **50**, 1218 (1994).

[26] A. Svensson, M. O. Krause and T. A. Carlson, J. Phys. B **20**, L271 (1987).

[27] H. P. Kelly, in *X-ray and Inner-Shell Processes*, AIP Conference Proceedings No. 215, edited by T. A. Carlson, M. O. Krause and S. T. Manson (AIP, New York, 1990), p.292.

[28] M. Seaton, Rep. Prog. Phys. **46**, 167 (1983).

[29] C. H. Greene and L. Kim, Phys. Rev. A **38**, 5953 (1988).

[30] J. P. Connerade and A. M. Lane, Rep. Prog. Phys. **51**, 1439 (1988).

[31] M. Ya. Amusia, *Atomic Photoeffect* (Plenum, New York, 1990).

[32] N. M. Kabachnik and I. P. Sazhina, J. Phys. B **9**, 1681, 1976

[33] U. Fano, Phys. Rev. **124**, 1866 (1961).

[34] P. Heimann (private communication).

[35] U. Becker, R. Hölzel, H. G. Kerkoff, B. Langer, D. Szostak and R. Wehlitz, Phys. Rev. Lett. **56**, 1120 (1986).

[36] B. Langer, N. Berrah A. Farhat, O. Hemmers and J. D.Bozek, Phys. Rev. A **53**, R1946 (1996).

[37] T. Manson and A. Starace, Rev. Mod. Phys. **54**, 389 (1982).

[38] P. G. Burke and K. T.Taylor, J. Phys. B **8**, 2620 (1975).

[39] N. Berrah, B. Langer, J. Bozek, T. W. Gorczcyca, O. Hemmers, D. W. Lindle and O. Toader, submitted to Phys. Rev. A.

[40] B. Crasemann, in *Atomic and Molecular Physics with Synchrotron Radiation*, edited by I. E. McCarthy, W. R. McGilliray and M. C. Standish (AIP, Brisbane, Australia, 1992) pp.69.

[41] G. S. Brown, M. H. Chen, B. Crasemann and G. Ice, Phys. Rev. Lett. **45**, 1937 (1980)

[42] H. Aksela, S. Aksela, O-P. Sairaren, A. Kivimaki, A. Naves de Brio, E Nommiste, J. Tulkki, S. Svenson, A. Ausmees and S. J. Osborne, Phys. Rev. A **49**, R4269 (1994).

[43] H. Aksela, et al., Phys. Rev. A **51**, 1291 (1995).

[44] Z. F. Liu, et al., Phys. Rev. Lett. 72, 621 (1994).

[45] W. Eberhard, G. Kalkhoffen and C. Kunz, Phys. Rev. Lett. **41**, 156 (1978).

[46] V. Schmidt et al., Phys. Rev. A **24**, 1803 (1981).

[47] H. Aksela et al., Phys. Rev. A **33**, 3867 (1986).

[48] U. Becker et al., Phys. Rev. A **33**, 3891 (1986).

[49] P. A. Heimann et al., J. Phys. B **20**, 5005 (1987).

[50] U. Becker et al., J. Phys. B **22**, 749 (1989).

[51] C. D. Caldwell, in *15th International Conference on X-Ray and Inner-Shell Processes*, edited by T. A. Carlsson, M. O. Krause and S. T. Manson (American Institute of Physics, Knoxville, 1990), pp. 685.

[52] T. A. Carlson et al., Phys. Rev. A **39**, 1170 (1989).

[53] J. W. Cooper, Phys. Rev. A **39**, 3714 (1989).

[54] B. Kämmerling, B. Krässig and V. Schmidt, J. Phys. B **23**, 4487 (1990).

[55] U. Hergenhahn, N. M. Kabachnik and B. Lohmann, J. Phys. B **24**, 4750 (1991).

[56] U. Hergenhahn et al., J. Phys. B **26**, L117 (1993); private

communication (1995).

[57] M. H. Chen, Phys. Rev. A **47**, 3733 (1993).

[58] J. Tulkki, H. Aksela and N. M. Kabachnik, Phys. Rev. A **50**, 2366 (1994).

[59] S. Masui et al., E. Shigemasa, A. Yagishita and I. A. Sellin, J. Phys. B **28**, 4529 (1995).

[60] J. E. Hansen and W. Persson, Phys. Scr. **36**, 602 (1987).